Chapter 2
OCT Technique – Past, Present and Future

Tigran Kostanyan, Gadi Wollstein, and Joel S. Schuman

Abstract Optical coherence tomography (OCT) has become the cornerstone technology in clinical and research imaging in the past two decades. OCT performs in vivo, real-time, noncontact scanning and provides cross-sectional and volumetric images with a resolution approaching that of histology. The technology is used in various medical disciplines, but it is still most profoundly used in the field of ophthalmology where it was initially applied. OCT is continuously evolving with newly developed applications.

This chapter will describe the basic principles of OCT techniques, its history, current status, and major ophthalmic applications and research that will determine the future of the technology.

Keywords Time domain (TD-) OCT • Spectral domain (SD-) OCT • Swept source (SS-) OCT • Polarization sensitive (PS-) OCT • Adaptive optics (AO) • OCT blood flow

Abbreviations

OCT	Optical coherence tomography
RNFL	Retinal nerve fiber layer
TD	Time-domain

T. Kostanyan, MD
Department of Ophthalmology, University of Pittsburgh School of Medicine, UPMC Eye Center, Eye and Ear Institute, Ophthalmology and Visual Science Research Center, Pittsburgh, PA 15213, USA

G. Wollstein, MD • J.S. Schuman, MD (✉)
Department of Ophthalmology, University of Pittsburgh School of Medicine, UPMC Eye Center, Eye and Ear Institute, Ophthalmology and Visual Science Research Center, Pittsburgh, PA 15213, USA

Department of Bioengineering, Swanson School of Engineering, University of Pittsburgh, Pittsburgh, PA 15213, USA
e-mail: schumanjs@upmc.edu

© Springer International Publishing Switzerland 2016

A. Grzybowski, P. Barboni (eds.), *OCT in Central Nervous System Diseases: The Eye as a Window to the Brain*, DOI 10.1007/978-3-319-24085-5_2

SD	Spectral domain
FD	Fourier domain
SS	Swept source
AO	Adaptive optics
PS	Polarization sensitive
2D	Two-dimensional
3D	Three-dimensional
CCD	Charge-coupled device
ONH	Optic nerve head
ILM	Internal limiting membrane
IS	Inner segment
OS	Outer segment
RPE	Retinal pigment epithelium
LC	Lamina cribrosa
RGC	Retinal ganglion cell
IPL	Inner plexiform layer
GCC	Ganglion cell complex
EDI	Enhanced depth imaging

2.1 Introduction

Optical coherence tomography (OCT) is a diagnostic imaging technology that has gained a leading position in research and clinical practice due to its ability to obtain noncontact, in vivo, high-resolution, micron-scale images of tissue structures. OCT makes *in situ* imaging of tissue microstructure possible with a resolution approaching that of light microscopy histology without the need for tissue excision and processing, referred to as *optical biopsy* [1].

The technology uses the principle of low-coherence interferometry, which was originally applied to ophthalmology for in vivo measurements of the axial length of the eye [2]. OCT has been used to visualize various types of biological tissue [1, 3–9], but it is most profoundly used in ophthalmology due to the almost perfect optical accessibility of the eye.

At the time of introduction, the technology was used to acquire in vivo cross-sectional images of the anterior segment [10], as well as retinal pathologies such as macular edema, epiretinal membranes, macular holes, macular detachment, and idiopathic central serous chorioretinopathy [11]. Optic disc and retinal nerve fiber layer (RNFL) measurements were obtained with OCT shortly afterward [12–14].

OCT has evolved significantly, with improvements in both imaging method and image analysis. The evolution of OCT began with the time domain (TD) technique, followed by spectral domain (SD) and later newer iterations with faster scanning aquisition speeds [15–17] and higher axial resolution [18, 19].

This chapter will describe the basic principles of OCT techniques, its history, current status, and major ophthalmic applications and research that will determine the future of the technology.

2.2 Basic Principles

OCT provides cross-sectional and volumetric images of areas of interest by acquiring either the echo time delay or frequency information of back-reflected light. Differences in the optical properties of biological tissues allow the recognition of layered structures. The speed of light makes it impossible to analyze the acquired information directly, since it would be in the order of femtoseconds, thus OCT systems use the optical technique known as *interferometry*. Low-coherence interferometry enables analysis of this information and the creation of a depth-resolved reflectivity profile (A-scan) of the scanned tissue by matching the light profiles from the scanning and reference arms.

Utilization of light provides OCT technology the ability to obtain images in a non-contact fashion and to achieve resolutions of 1–15 μm, which is one to two orders of magnitude finer than other conventional clinical imaging technologies such as ultrasound, computerized tomography, or magnetic resonance. Light is highly absorbed or scattered in most biological tissues, and therefore the use of this technology is limited only to locations that are optically accessible or that can be imaged using devices such as endoscopes or catheters.

OCT technique can be classified into two major groups: TD and Fourier (or frequency) domain (FD). FD can be further classified into spectral-domain (SD) and swept-source (SS) techniques. In TD-OCT, a broad-bandwidth laser or a low-coherence superluminescent diode light source projects light that is then divided into two arms by a partially reflecting mirror (beam splitter). In the first arm light is projected toward the sampling location, while in the second arm light is projected toward a moving reference mirror at a known position. The backscattered light from both sites travel back to a detector and recombine to form an interference pattern, which is sensed by the interferometer. The interference is only observed when both the sample and the reference arm light beams travel the same distance [12]. Changing the position of the reference mirror allows the machine to sequentially acquire information from different depths in the tissue sample. A cross-sectional image, also known as a B-scan, is generated by performing fast, subsequent axial scans (A-scans) at different transverse positions. Each axial scan represents the echo time delay of back-reflected light from the tissue and gives a profile of the tissue's dimensions along the optical beam. The scanning speed of TD-OCT technology is limited to 400 axial scans/sec, due to the maximal oscillating speed of the reference mirror [20].

SD-OCT is similar in principle, but the data acquisition varies slightly, yet fundamentally, from TD-OCT. The main difference of this iteration is the use of light frequency information instead of time delay data to determine the spatial location of reflected light. SD technology utilizes the Fourier transformation of the reflected light frequencies to encode distances within tissue microstructure [21]. Instead of a moving reference mirror, the mirror is stationary and the interference signal is split into its frequency components using a diffraction grating. The signal is simultaneously detected by a charge-coupled device (CCD). The CCD has an array of photodetectors that are each sensitive to a range of specific frequencies [22, 23].

SD technology allows the acquisition of information from all points along each A-scan simultaneously, substantially increasing scan speed to the range of ~25,000–

75,000 axial scans/sec in the commercially available systems [24, 25] and up to 20.8 million axial scans/sec in research devices [16]. The substantial increase in scanning speed allows for the acquisition of three-dimensional (3D) data sets, which is done by combining rapidly acquired subsequent cross-sectional scans. The wide bandwidth of the light source also enables a substantial enhancement in axial resolution up to 1 μm [26, 27] and an improved signal-to-noise ratio [28].

SS-OCT is a form of Fourier domain technology that uses a single tunable laser that sweeps through different frequencies to rapidly cover the entire broad spectrum. The reflectance of the light from the scanned area is captured by a photodetector, which is much faster than the CCD camera used in SD-OCT technology [17, 29]. This allows the SS technology to further enhance the scanning speed up to 400,000 axial scans/sec. Another important advantage of this iteration of OCT technology is the absence of the depth dependent signal drop-off observed with SD-OCT technology [30]. Most SS-OCT devices operate with light sources centered at around 1030 μm (compared with 840 μm in the commercially available TD- and SD-OCT), which reduces the axial resolution to approximately 8 μm but allows for better penetration of the tissue. The combination of improved tissue penetration and reduced signal attenuation allow detailed scanning of structures such as the choroid and the lamina cribrosa inside the optic nerve head. The major characteristics of these three different OCT techniques are presented in Table 2.1.

The key technological parameters that are typically used to characterize OCT technology are the wavelength of the light source, axial or longitudinal resolution,

Table 2.1 Comparison of TD-, SD-, and SS-OCT technologies

Technology	Light source	Ophthalmic device commercially available	Primary advantages	Primary disadvantages
TD-OCT	Relatively narrow band width	Yes	Intensity information acquired in time domain; no complex conjugate image	Moving reference mirror required, limiting acquisition rate
SD-OCT	Broadband width	Yes	No moving reference mirror required; higher resolution than TD-OCT; high scanning speed and axial resolution can be attained	Noticeable signal drop-off with depth
SS-OCT	Narrow band, swept through broad range	Yes	No moving reference mirror required; very high scanning speeds can be attained; minimal signal drop-off with depth	Most ophthalmic systems are operating at longer wave lengths ($\lambda = 1–1.3$ μm) with lower axial resolution than SD-OCT but with improved penetration into structures

lateral or transverse resolution, scanning speed, and imaging depth. The wavelength is inversely related to the axial resolution of the acquired images, with longer wavelength providing lower resolution compared with shorter wavelength.

Axial resolution determines the smallest distance along the axial direction where two adjacent points are discernable, and it is related to the bandwidth or the coherence-length of the source. In posterior segment eye imaging, the light should travel through transparent media, which mostly contains water that absorbs infrared radiation. This limits the technology to the use of light sources of only certain wavelength. Current commercial OCT devices achieve axial resolutions up to 4 μm, and research systems achieve up to ~ 1–2 μm [19].

Transverse resolution is independent of the coherence properties of the light source, and is determined by the spot size, which is limited by the optics of the scanned system. As such, the transverse resolution of OCT among the different generations is within a range of 15–20 μm. Improving the transverse resolution requires the correction of the optical aberrations of the eyes using technologies such as adaptive optics.

Scanning speed is dictated by mechanical constrains such as the maximal oscillating rate of the reference arm (TD-OCT) and the sensitivity of the detector to the back-reflected light. As scanning speed increases, the time the detector remains in the same location is shorter, thus reducing the light that can be detected in each location. Since the power of the projected light is limited in order to be within safety limits, faster scans require a more sensitive detector that can function with a lower level of light.

The imaging depth in TD technology is given by the reference arm's range of movement, while in SD technology it is related to the center wavelength. Longer wavelengths provide increased imaging depth [31, 32], but the use of longer wavelengths for imaging depth improvement is limited by the increased optical absorption of water [33].

2.3 The Past

OCT technology was first described by Huang and colleagues in 1991 [34]. The authors scanned human retinas and atherosclerotic plaques ex vivo with a prototype device using infrared light at a ~ 800-nm wavelength. The axial resolution of cross-sectional images of the retina, optic nerve, and coronary artery wall was 15 μm, which allowed the visualization of some retinal layers, optic nerve head structures, and the composition of the coronary artery. In vivo retinal scanning was conducted using a prototype device based on a slit-lamp biomicroscope that was modified to provide a view of the fundus while scanning with OCT. The development of scan patterns that enabled the acquisition of reproducible measurements [35] led to the use of the technology in clinical practice.

The first commercially available OCT, called OCT 1000, was marketed in 1996 by Zeiss (Dublin, CA). The technology went through two iterations, resulting in OCT 2000 in the year 2000 and then OCT three (Stratus OCT), which became commercially available in 2002. The Stratus OCT had an axial resolution of ~10 μm, a

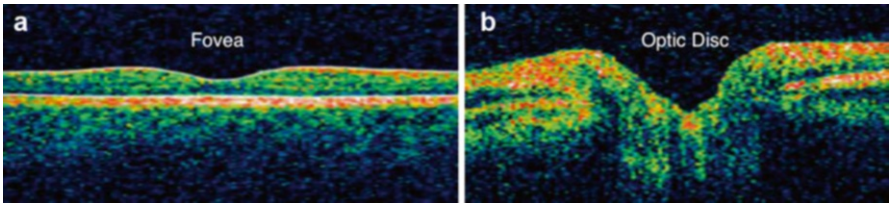

Fig. 2.1 OCT image of a healthy fovea (**a**) and optic disc (**b**). Images were obtained using TD technology and have an axial resolution of ~10 μm

transverse resolution of 20 μm, and a scan speed of 400 axial scans/sec [1, 12]. The typical cross-sectional scan was composed of 128–512 axial scans, comprising an image area of 4–6 mm.

Due to its ability to obtain quantitative and reproducible measurements of the macula [36, 37], retinal nerve fiber layer thickness [35, 38], and optic nerve head [39, 40], TD-OCT technology became the gold standard in-vivo clinical imaging device for posterior segment pathologies in a relatively short period of time. Figure 2.1 shows an example of a cross-sectional scan of the macula and the ONH of a healthy eye obtained with TD technology (Stratus OCT).

The most routine scan patterns used with TD-OCT were a scan comprises of six equally spaced radial scans through the macula (6 mm diameter) and optic nerve (4 mm) and a circular scan with a diameter of 3.4 mm centered on the optic nerve head (ONH). Using automated segmentation, the macular thickness (internal limiting membrane (ILM) to the photoreceptor inner segment-outer segment (IS–OS) junction) can be quantified from the macular scan pattern, and the retinal nerve fiber layer (RNFL) thickness measurements can be quantified from the circumpapillary scan. Cup area, disc area, cup diameter, disc diameter, and rim area are provided after the software detects the ONH margin, allowing quantification of the ONH.

Several improvements in OCT hardware have been introduced since the first commercial TD-OCT system became available. Better axial resolution [26, 27] and increased scanning speed [22, 41] are the two main advancements that were incorporated into the commercial systems. Ultra-high resolution OCT retinal imaging that used specially designed broadband light sources was introduced in 2001 [42]. This OCT device had an axial resolution of ~3 μm, which was markedly better than the 10 μm axial resolution provided by the commercial devices at that time [42, 43]. Further improvements in OCT technology lead to the introduction of SD-OCT (discussed in detail in the next section) which had a faster scanning speed and better resolution than TD-OCT. This can be easily appreciated by comparing Figs. 2.1 and 2.2, in which the same healthy eye was scanned with TD- and SD-OCT, respectively.

In addition to acquiring tissue structural information, OCT has been incorporated into multimodal imaging systems that provide further insight into the functional characteristics of tissue [44–50].

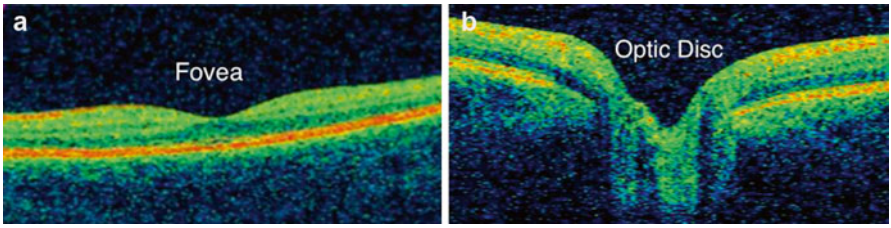

Fig. 2.2 OCT image of a healthy fovea (**a**) and optic disc (**b**). Images were obtained using SD technology and have an axial resolution of ~5 μm

2.4 The Present

OCT has become a key ophthalmic diagnostic imaging tool due to its ability to provide reliable and reproducible information about tissue microstructure. The majority of current commercial OCT systems use SD technology for posterior eye imaging and can visualize the cross-sectional structure of the retina and optic disc [1, 51]. OCT is used extensively in the diagnosis and management of a wide range of ocular pathologies including glaucoma, age-related macular degeneration, macular edema, macular holes, diabetic retinopathy, alterations in the vitreoretinal interface, papill-edema, and others. OCT systems possess different built-in scanning protocols for obtaining data on macular, peripapillary, and optic disc structures. In addition to providing a cross-sectional and volumetric dataset of the scanned area, individual layers and structures of the retina and optic disc are measured by automatic image processing. In many devices, these measurements are compared to normative data acquired from the population, with some devices also factoring in ethnicity. The comparison with normative data simplifies the recognition of abnormal locations. The ability of OCT to provide reproducible, quantitative information makes it useful in tracking small changes in tissue structure along the course of disease.

Some scan patterns used in SD-OCT are similar to those described above for TD-OCT, but a dramatic increase in scanning speed substantially extended the abilities of SD-OCT. SD-OCT is able to acquire a larger number of axial scans or transverse pixels per image, as well as a larger number of cross-sectional images for a given scan time, which results in improved image quality and retinal coverage. The faster scanning speed reduces eye motion artifacts, due to the shorter acquisition time, and improves the accuracy of the acquired images. The faster scanning speed also enables the acquisition of a 3D volumetric dataset in a time comparable to that of the scanning protocols of previous generations OCT. A 3D dataset allows a thorough sampling of the scanned region, advanced post-processing, and improved registration of consecutive scans. One of the common uses of the advanced processing is the OCT en face image generated by integrating each individual axial-scan [52]. The en face image is similar to the conventional retinal fundus view and can be used for subjective assessment of image quality, comparison with clinical findings, and to assist with correcting eye motion that may have occurred during the scan. The en

face view can be used to further focus on slab within the region of interest, allowing detailed visualization of structures such as the fine intra-retinal vascular network.

Evaluation of the ONH using SD-OCT can provide important diagnostic information in multiple ocular and central nervous system pathologies. Figure 2.3 shows an OCT cross-sectional image of a healthy optic disc (a) and a 3D volumetric scan (b).

ONH imaging is performed using different scan patterns among the various commercially available SD-OCT devices. This includes 3D cube scans, radial scans, circular scans, and a combination of radial and concentric scans. The 3D volumetric cube is obtained by the raster scanning of a square area centered on the ONH. The radial scan is composed from various numbers of cross-sections at equal angular orientation all centered on the ONH. Circular scans are centered at the ONH, similar to the scan pattern performed with TD-OCT. A scan that is a combination of a radial and concentric scan is beneficial because it features dense sampling adjacent to the intersection of the radial scans while the circular scanning at the periphery fill in the gaps between the radial scans that are further out from the intersection. All of the devices can automatically detect the optic disc boundaries from each acquired image as the location at which the photoreceptor layer, retinal pigment epithelium (RPE), and choriocapillaries terminate.

One of the most useful measurements provided by OCT is the circumpapillary RNFL thickness, which quantifies the retinal ganglion cell's axons from the entire retina on their way toward the ONH. This measurement can be extracted from a circle centered on the ONH with a diameter of 3.4 mm, similar to the method used in TD-OCT. The limitation of this approach is that the sampling of the tissue is performed only along the circle, and therefore any misplacement of the circle during repetitive scanning will result in increased measurement variability.[53] Another option is to extract the RNFL thickness from the 3D cube scanning pattern. This

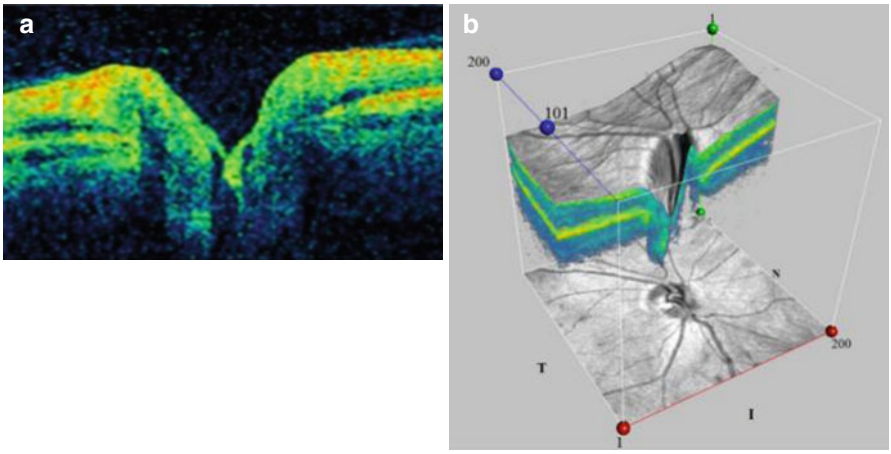

Fig. 2.3 Cross-sectional (**a**) and volumetric (**b**) SD-OCT imaging of the optic nerve head of a healthy eye

method can ensure that the tissue sampling location is consistent through multiple scans, as the repositioning of the circle is possible if needed.

SD-OCT devices provide average RNFL thickness measurements, thicknesses in four quadrants (temporal, superior, nasal and inferior) and sectoral thicknesses at each of the 12 clock-hours or in 16 equal sectors. The RNFL thickness profile in the peripapillary region follows the ISNT rule, with thickest RNFL seen in the inferior quadrant, followed by superior, nasal and temporal quadrants.

Several devices also report the RNFL thickness as a color-coded thickness map of the entire peripapillary region. This map provides additive information to the circumpapillary RNFL thickness, as it can highlight small, localized thinning or defects outside the circumpapillary sampling location.

Figure 2.4 shows Cirrus HD-OCT ONH scan printout that provides the RNFL thickness map (a) and cross-section (c). The deviation map (b) compares the RNFL measurements at each superpixel with an age-matched normative database, and locations thinner than the lower 95 % of the normal range are highlighted. At the

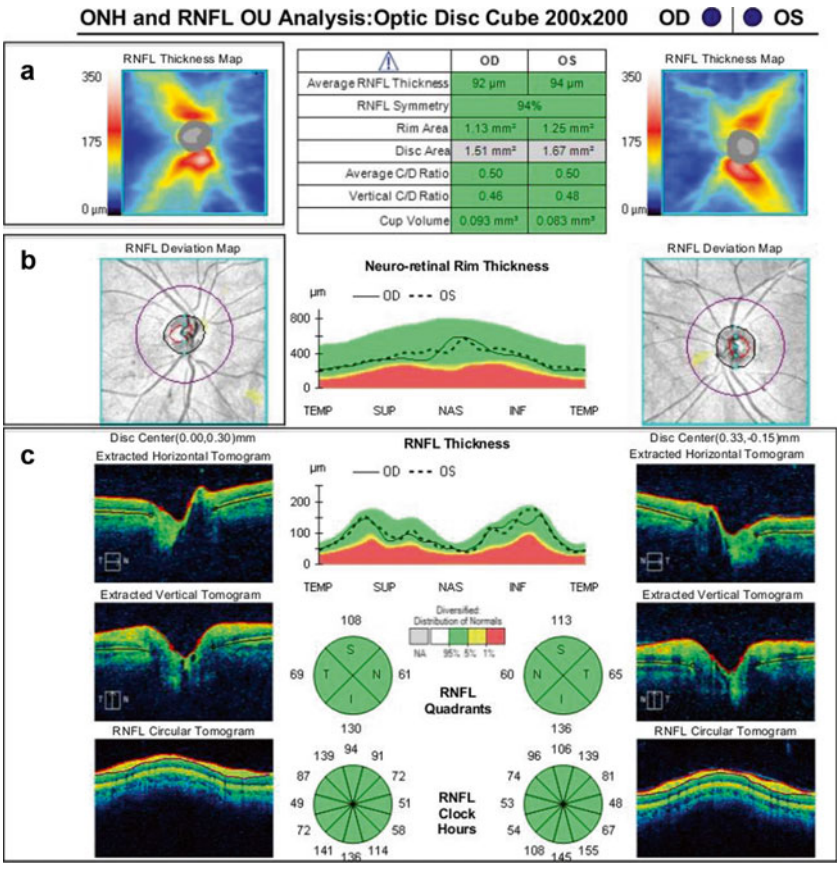

Fig. 2.4 Cirrus HD-OCT ONH scan printout with RNFL thickness map (**a**), deviation map (**b**) and cross section (**c**)

center panel quantitative parameters are provided for ONH structures, along with RNFL thickness. The background coloring reflects the comparison with the normative results, with green representing the normal range, yellow representing <5 % of the normal population, and red representing and <1 %.

Figure 2.5 demonstrates the circumpapillary RNFL scans obtained with the Spectralis OCT (a). Spectralis measure RNFL thickness by assessing a total of 2,325 data points along the sampling circle, and the built-in software constructs the final cross-section by averaging 16 consecutive B-scans. The averaging of multiple scans reduces the background noise and improves signal quality. The actual thickness values and color-coded comparison results are presented as global average thickness, thickness in four quadrants, and thickness in six sectors (b).

The RTVue Premier peripapillary scan acquire 13 circular scans with diameters of 1.3–4.9 mm centered on the ONH. The comparison with the normative database is performed in 16 sectors and presented as the deviation map that surrounds the RNFL thickness map in Fig. 2.6a.

The improvements introduced in SD-OCT had a substantial impact on macular imaging. Thorough sampling of the macula, the improved visualization of the retina and choroid, and the ability to automatically segment the various layers of the retina substantially impacted clinical management. The scan patterns that are often used to image the macula include the 3D cube, line and cross-line, raster, mesh, and radial scan patterns. The principle of the volumetric cube scan is similar to the 3D ONH scan patterns described above.

Figure 2.7 shows a macular 3D scan obtained with Cirrus HD-OCT (a) and Spectralis OCT (b) from two different healthy subjects. These types of scans are

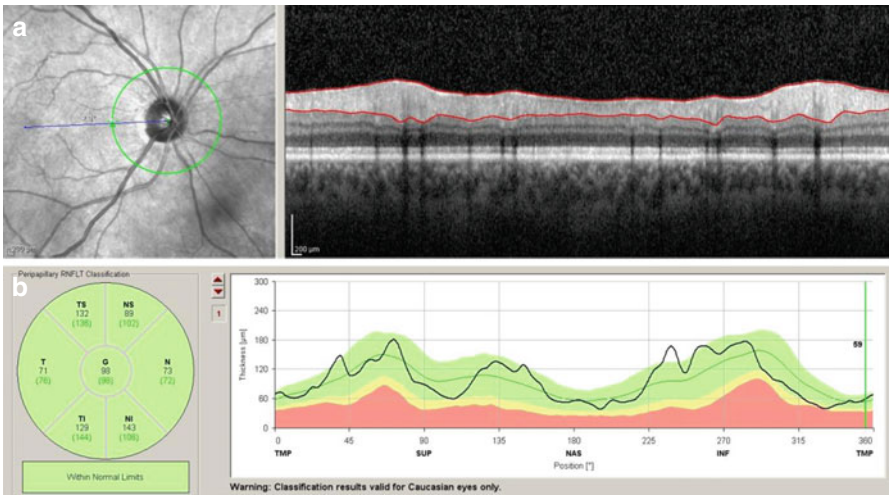

Fig. 2.5 Spectralis OCT RNFL Analysis with circumpapillary RNFL cross section (**a**), thickness profile and sectoral measurements (**b**)

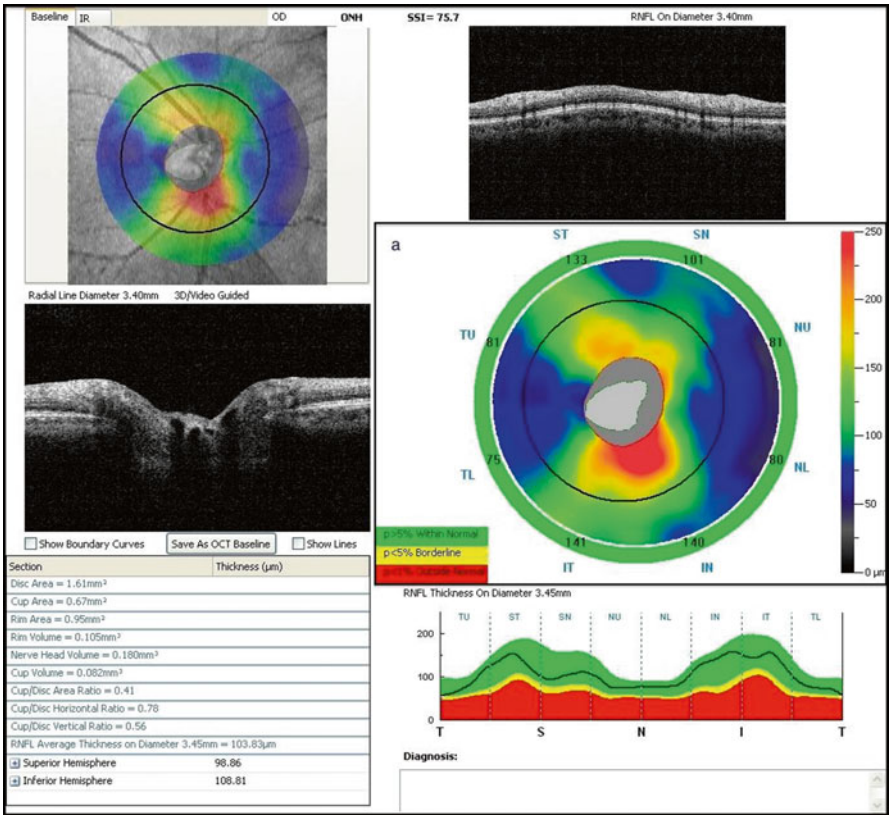

Fig. 2.6 ONH and peripapillary RNFL thickness protocol of RTVue premier

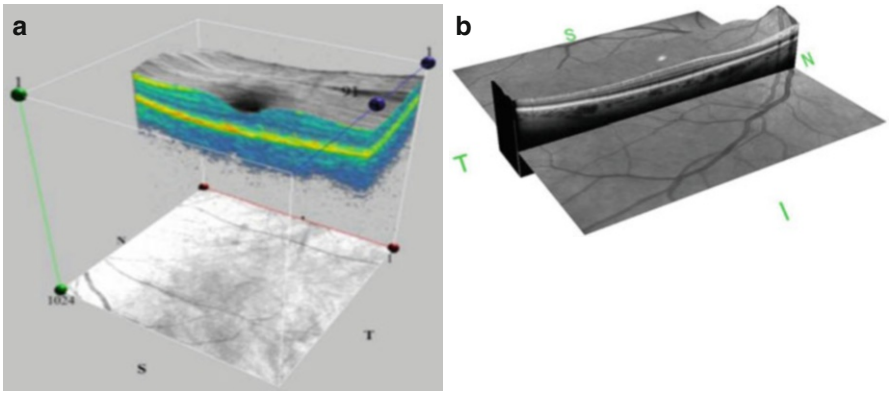

Fig. 2.7 3D-OCT images of healthy maculas obtained with Cirrus HD-OCT (**a**) and spectralis OCT (**b**)

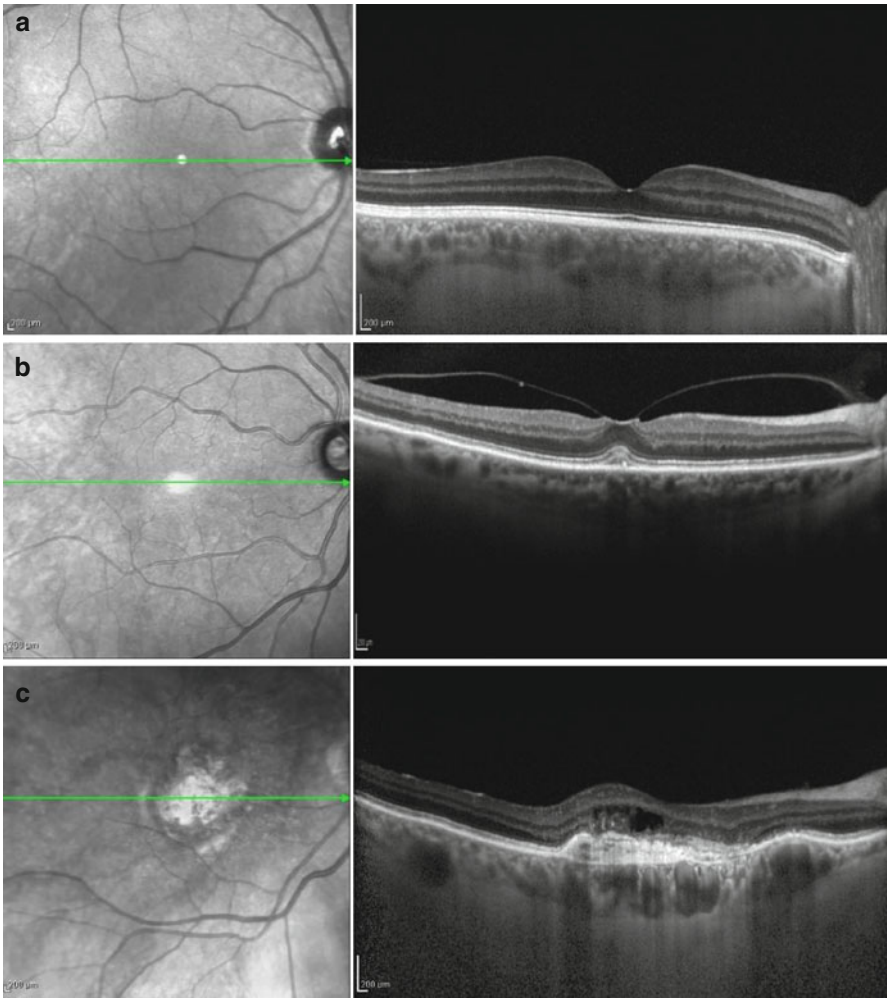

Fig. 2.8 Line scans of the macular region obtained with spectralis OCT from a healthy eye (**a**), and eyes with vitreomacular traction (**b**) and wet age-related macular degeneration (**c**)

often helpful in the estimation of the volume and extent of pathologies in the macula, such as macular edema or macular holes.

Line scans are typically composed from the averaging of multiple scans at the same location, as explained above. This is typically performed along a single location (Fig. 2.8) or along several parallel lines (Fig. 2.9). Line scans are clinically useful for obtaining retinal images with highest level of detail.

Some SD-OCT systems are capable of acquiring scans in horizontal and vertical orientations to provide a mesh scan pattern. The logic behind this scan pattern is that even at a fast scanning rate there is a relatively long temporal gap between adjacent points that are perpendicular to the scan orientation. For example, in a horizontal

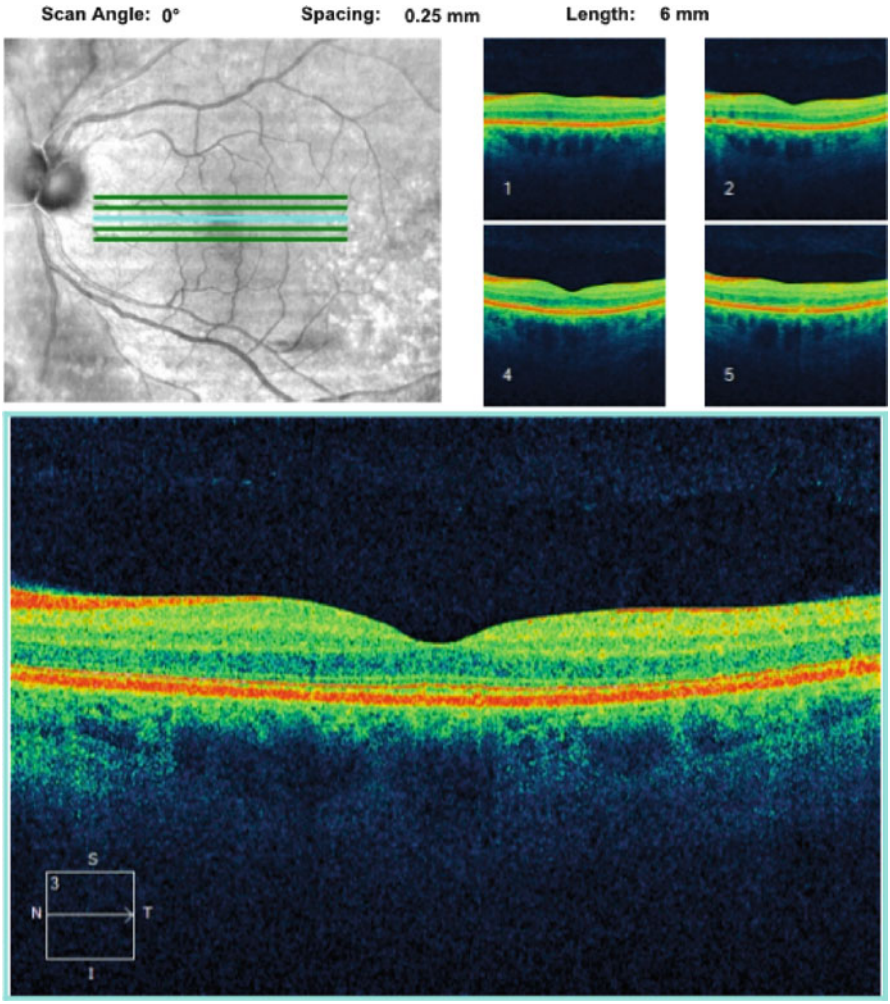

Fig. 2.9 Macular five line raster scanning pattern obtained with cirrus HD-OCT

raster scan, the time gap between adjacent points in the horizontal direction is much shorter than the gap between adjacent points vertically. This can lead to image distortion along the slow axis of the scan. Registering the horizontal and vertical scans together can reduce the distortion in the slow axis and improve scan quality. Figure 2.10 shows a mesh scanning pattern (b) of the macula centered on the fovea with correspondent cross-sectional image (a) obtained with RTVue Premier. The pattern consists of an inner, dense grid and outer grid, visible as white grid lines.

Radial scan protocols acquire multiple evenly spaced linear scans which all intersect at the fovea. This pattern provides information from the entire macular region, with dense coverage near the fovea where the lines intersect and sparse coverage at the macula periphery. Figure 2.11 demonstrates a radial scanning pattern of

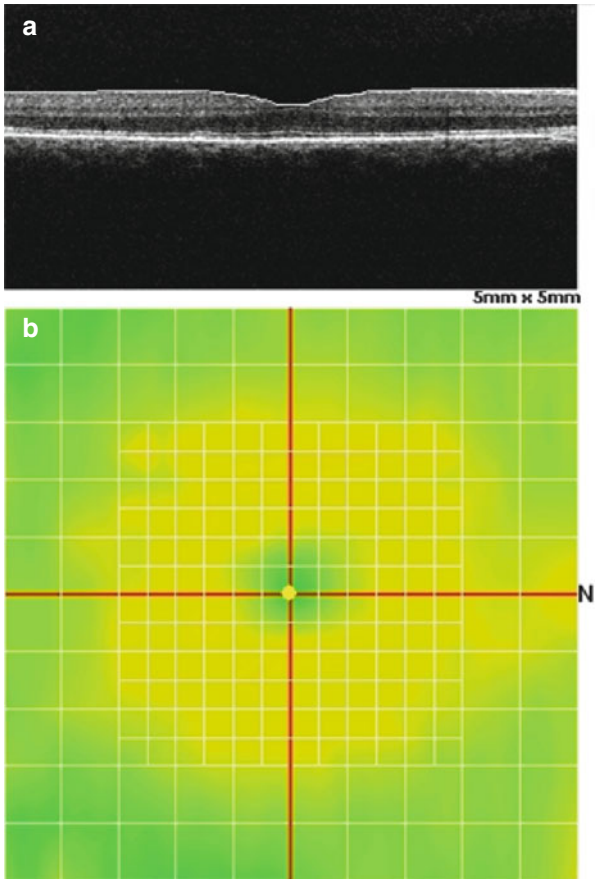

Fig. 2.10 Macular mesh scanning pattern (**a**) obtained with RTVue Premier and (**b**) with corresponding cross-sectional image

the macula from two different healthy subjects using different commercial SD-OCT systems.

The high resolution of SD-OCT allows the acquisition of reproducible segmentation and the analysis of individual macular layers that are of particular diagnostic interest [54, 55]. It has been suggested that three innermost retinal layers: the nerve fiber layer, the retinal ganglion cell (RGC) layer, and the inner plexiform layer (IPL) are directly prone to glaucomatous damage [56]. Cirrus HD-OCT extracts the information from an ellipse (vertical radius of 2 mm, horizontal radius of 2.4 mm) centered on the fovea and provides a combined measurement that includes RGC layer and IPL. The macula protocol of RTVue Premier provides the ganglion cell complex (GCC) that includes the macular NFL, RGC layer, and IPL. The data is captured from a 7 mm^2 area centered 1 mm temporal to the fovea (Figs. 2.12 and 2.13).

Enhanced depth imaging (EDI) is a scanning protocol that allows the acquisition of images from deeper ocular tissues. This method switches the point of maximal focus in the interference signal so that it is centered on deeper tissues. The advantages of this method have been shown in the visualization of the choroid [57], optic nerve head [58], and deeper structures within the optic nerve such as the LC [59].

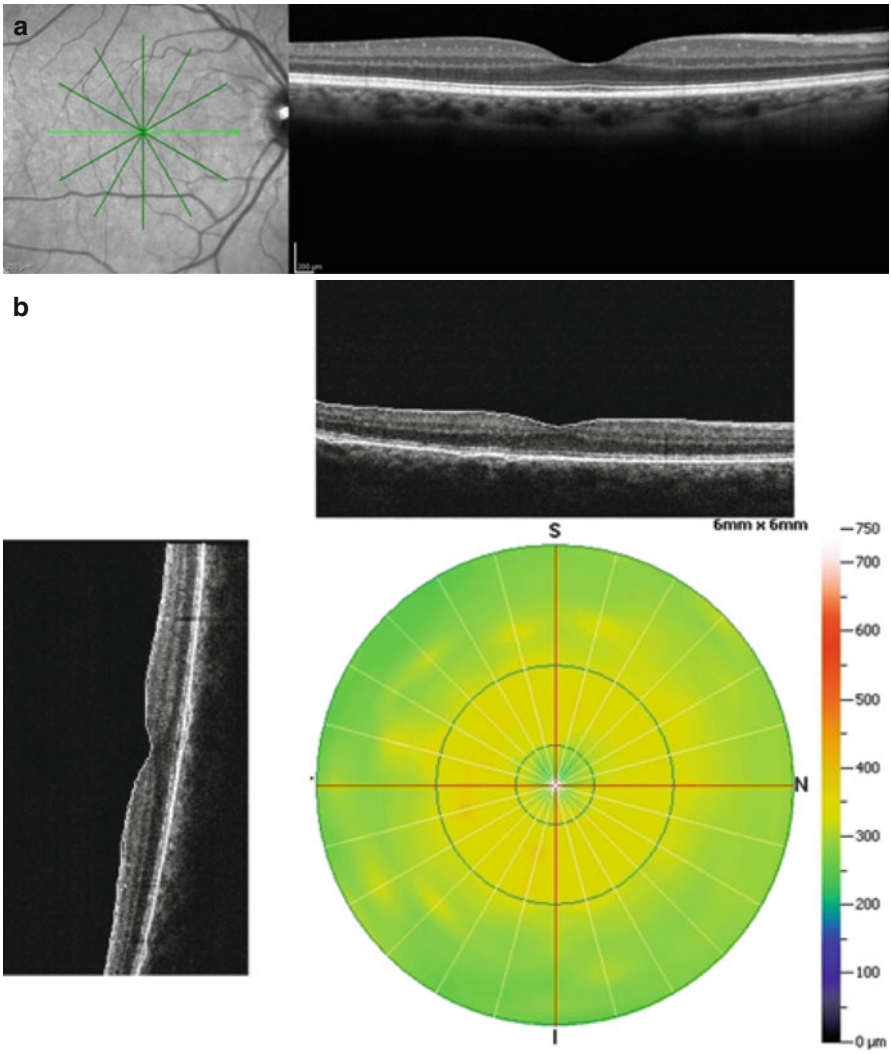

Fig. 2.11 Macular radial scanning pattern obtained with spectralis OCT (**a**) and RTVue premier (**b**)

Because OCT provides highly reproducible micron scale measurements, small structural changes occurring over time due to disease deterioration can be detected. Several commercial SD-OCT devices include a progression analysis tool. Automatic progression algorithms utilize trend-based analysis methods, primarily linear regression analysis, for computing the rate of change in structural parameters over time. The computed rate is compared to a no change slope to determine if the rate is statistically significant. This rate of change is also used to predict future progression beyond the most recent visit. This prediction can be useful when discussing disease forecast with a patient or to assess the effect of treatment modification. Several

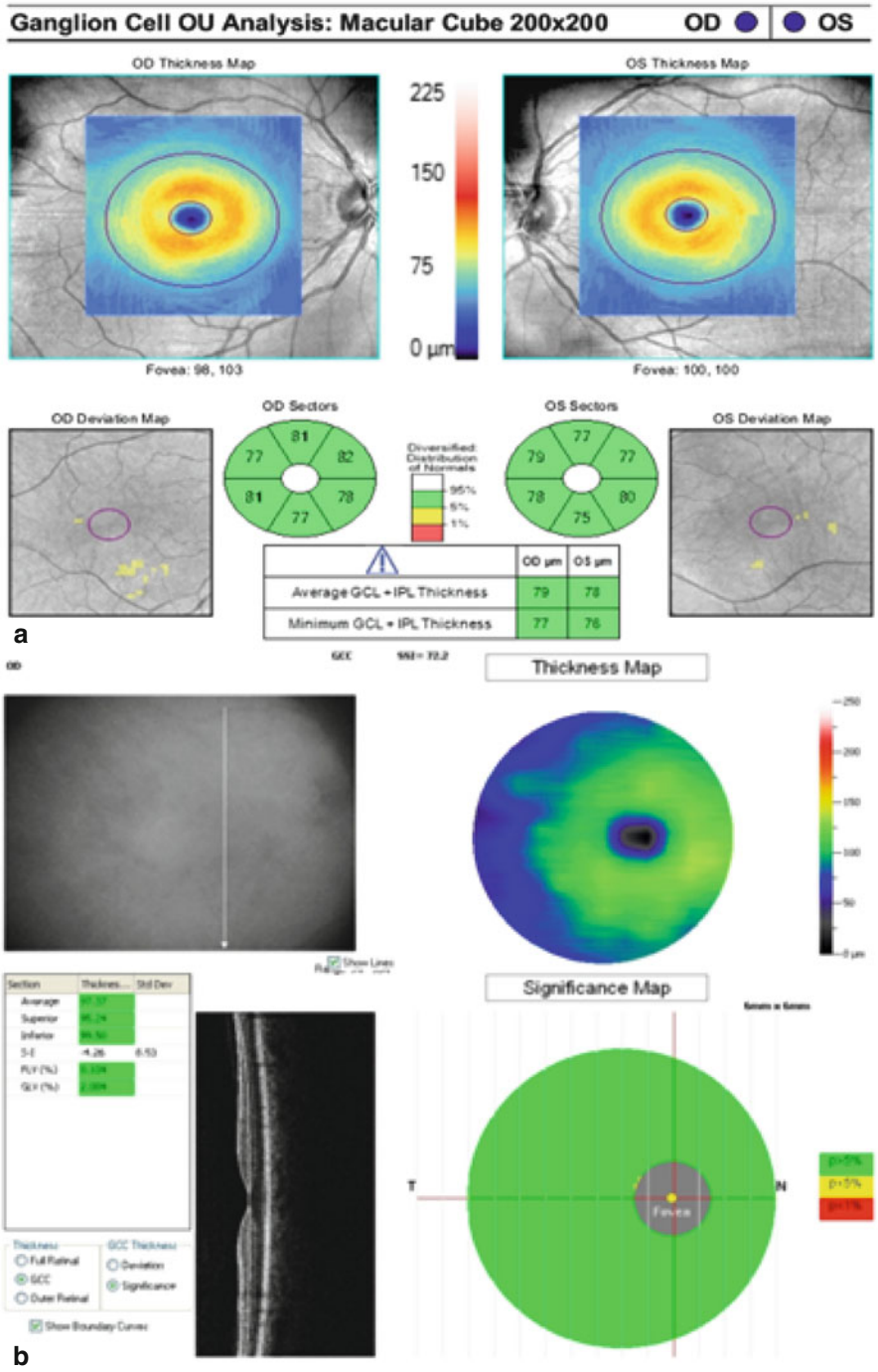

Fig. 2.12 Cirrus HD-OCT ganglion cell analysis (**a**) and RTVue premier GCC analysis (**b**)

commercial devices also provide event-based analysis, where a series of follow up measurements are compared with baseline measurements and progression is defined when measurements exceed a predetermined threshold for change from baseline.

2.5 The Future

As OCT technology keeps rapidly evolving, at the time of this writing several innovative OCT technologies are being tested. The following sections will provide a brief description of some of the most promising developments.

2.6 Swept Source OCT

As previously discussed, SS-OCT is a form of Fourier domain technology that obtains time-encoded spectral information by sweeping a narrow-bandwidth laser through a broad optical spectrum. This method uses a narrow-bandwidth light source and photodetector, in contrast to SD-OCT, which applies a broad bandwidth light source and detects the interference spectra with a CCD camera and spectrometer. The use of a photodetector allows SS-OCT to achieve higher scanning speeds and better sensitivity with imaging depth (Fig. 2.14) [17, 29, 60]. While SD-OCT suffers from signal attenuation along the axial path, SS-OCT is less prone to this effect, maintaining good imaging quality throughout the axial path. In addition, many SS-OCT systems use a light source centered at a ~1050 nm wavelength, allowing for better tissue penetration than SD-OCT, which typically uses a light source centered at ~840 nm. This enables visualization of structures such as the choroid (Fig. 2.15) [61, 62] and lamina cribrosa (LC) (Fig. 2.16) [63, 64] along with structures at the anterior segment of the eye [65]. Increased scanning speed results in a shorter scanning time and the reduction of image distortions caused by motion artifacts, which results in improved scan quality and better visualization of fine structures [15, 66]. These properties can improve visualization of retinal sub-RPE pathologies such as central serous chorioretinopathy, AMD, choroidal tumors, and retinitis pigmentosa [67].

The only commercially available anterior segment SS-OCT device (CASIA SS-1000, Tomey, Nagoya, Japan), at the time of this writing, provides automatic measurements of anterior chamber structures [68]. Examination of the LC and posterior sclera might improve the understanding of the mechanical aspects of glaucoma pathogenesis [69, 70].

The fast scanning speed of the SS-OCT allows the acquisition of widefield scans covering large areas of the fundus [71]. Another investigative development is a scanning method that allow the acquisition of data from the entire eyeball, from the cornea to the retina [72]. The clinical utility of all these features is still under investigation.

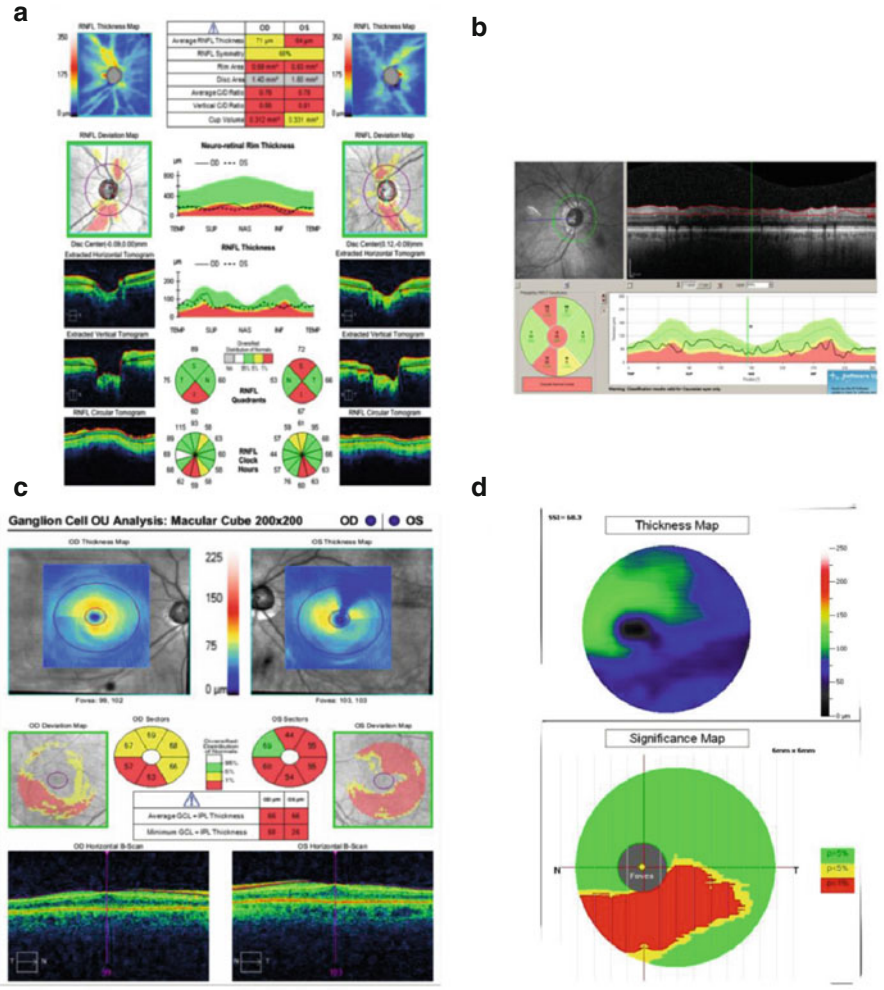

Fig. 2.13 Automated analysis for the detection of glaucomatous retinal and optic nerve damage provided by cirrus HD-OCT in the ONH region (**a**) and macula (**c**), spectralis OCT of the ONH (**b**), and RTVue premier of the macula (**d**)

2.7 Adaptive Optics

Adaptive optics (AO) is an optical method designed to dynamically adjust monochromatic aberrations in optical systems. AO was initially used in astronomy for correcting distortions of light passing through the atmosphere. The first in vivo examination of the retina with an AO fundus camera using a Hartmann-Shack wavefront sensor and a deformable mirror was introduced in 1997 [73]. A few years

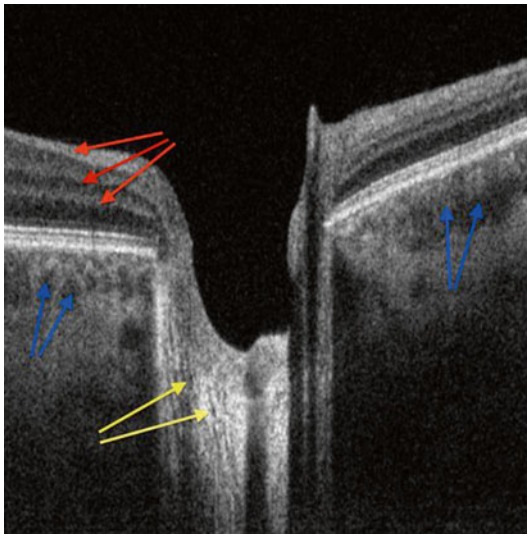

Fig. 2.14 Swept-source OCT cross section. The same scan can capture retinal layers (*red arrows*), nerve fiber fascicles passing through lamina cribrosa (*yellow arrows*), and choroidal vessels (*blue arrows*) because this technology is less prone to signal drop-off in comparison with other OCT iterations

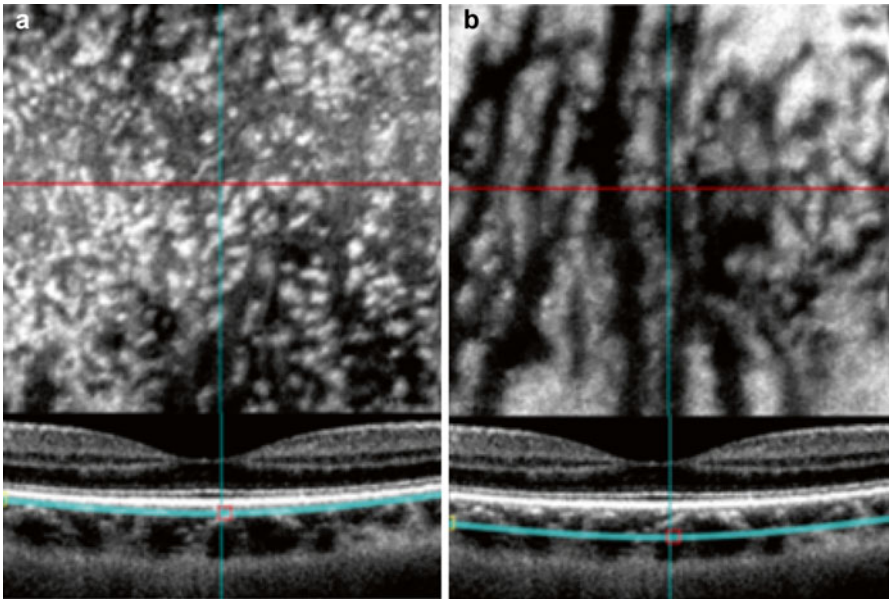

Fig. 2.15 Swept-source OCT macular cross-section. The upper panel of the figure demonstrates en-face image of choriocapillaries (**a**) and choroid (**b**) with correspondent cross-sectional scans at the bottom panel. The thick turquoise line in the cross-section images marks the plane where the en-face is acquired

later, AO was combined with scanning laser ophthalmoscope [74] and OCT systems [75, 76]. The transverse resolution of all conventional OCT systems is limited to the range of 20 μm due to the optical aberrations of the light beam when passing through

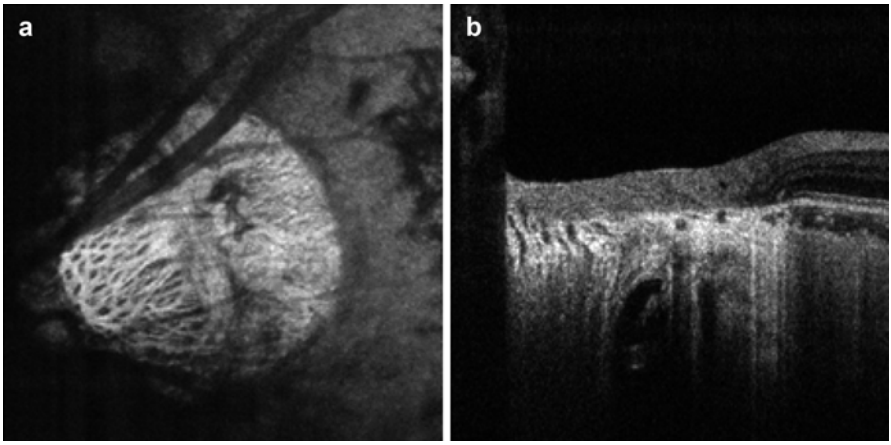

Fig. 2.16 Swept-source OCT lamina cribrosa en-face and cross-section. En-face image (**a**) of lamina cribrosa demonstrating the intricate structure of the hyperreflective beams (*white*) and hyporeflective pores (*black*) with corresponding cross-sectional scan (**b**)

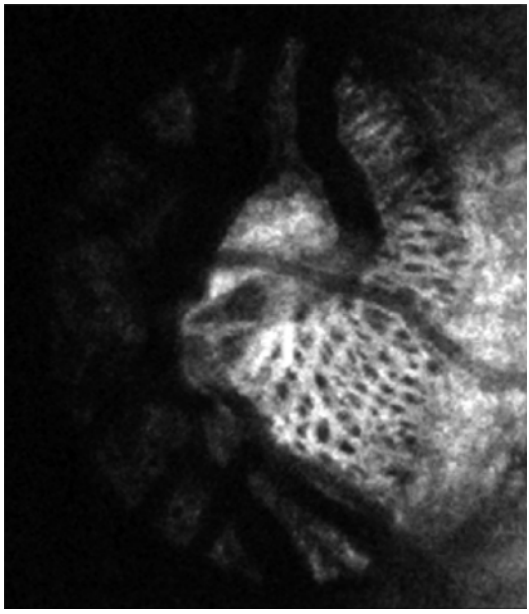

Fig. 2.17 Adaptive optic SD-OCT en-face lamina cribrosa image demonstrating the highly detailed visualization of this complex structure

various media in the eye. AO measures and corrects the optical aberrations, reduces the projected spot size, and improves the transverse resolution to the range of 5–10 μm [75]. This resolution allows the acquisition of highly detailed images, enabling the visualization of fine details such as the retinal microvasculature, photoreceptor mosaic [77], LC (Fig. 2.17), and microstructures within the RNFL [18, 78] and ganglion cell layer. The ability to acquire highly detailed in vivo images of

these structures allow further insight into ocular anatomy in health and disease, providing the opportunity to expand the understanding of pathologic processes in the eye.

The major limitation of the AO technique is the small field of view, which is restricted to approximately 1° to 3°. The use of an eye-tracking system to acquire a series of neighboring scans to cover a larger volume might resolve this limitation, though the longer scanning time might prohibit large scale clinical use [79]. Similarly, the focusing depth of the AO technique is also limited, and therefore acquiring high quality images of structures such as the choroid and retina in the same image is difficult to obtain. It may be possible to address this limitation by varying the focal plane while scanning in depth [80, 81].

2.8 Polarization Sensitive OCT

Polarization sensitive OCT (PS-OCT) uses the polarization state of polarized light for the assessment of tissue function [44]. Different ocular structures and tissues alter the polarization state of light in different ways, such as through birefringence (sclera, RNFL), polarization-preservation (photoreceptors), and depolarization (RPE) (Fig. 2.18). PS-OCT estimates these light state alterations by simultaneously measuring intensity, retardation, and optic axis information, thus providing both tissue structural and functional information. The technology was initially incorporated

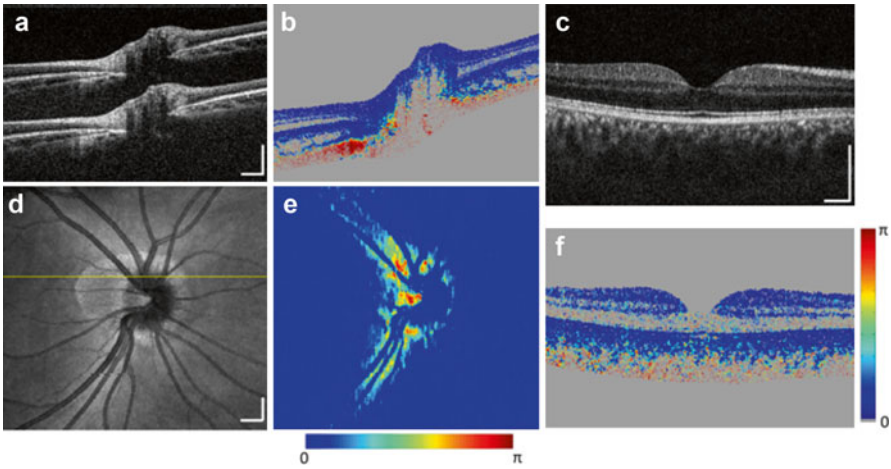

Fig. 2.18 PS-OCT optic nerve head and retinal imaging in healthy subjects. (**a**) A cross-sectional intensity image with two depth-encoded copies of the optic nerve head region. (**b**) Corresponding PS-OCT image shows high retardance in the RNFL and sclera. (**c**) OCT fundus image. (**d**) Corresponding PS-OCT map shows high retardance around the optic nerve head region. (**e**) A cross-sectional intensity image at the fovea region. (**f**) Corresponding PS-OCT image shows low retardance in the retinal layers. Scale bar: 500 μm

into TD-OCT system, with subsequent introduction into all known OCT iterations such as SD-OCT [49], SS-OCT [50], and AO-OCT [82]. Recent studies demonstrated that functional alteration in ocular tissues might precede the occurrence of structural alteration, and thus evaluation of the functional properties of the RNFL [83], sclera [84], and RPE [85, 86] using PS-OCT technology could be an attractive candidate for improving the detection of ocular pathologies such as glaucoma and age-related macular degeneration.

2.9 OCT Blood Flow and Angiography

Other methods of estimating the functional characteristics of tissue using OCT are Doppler OCT and OCT angiography [87].

Doppler OCT (Fig. 2.19) uses the information from the shift of light's optical frequency when it scatters from moving red blood cells. Two approaches have been taken to measure absolute blood flow: (1) post processing techniques to determine directionality of the vessels and than extract the moving signal from the blood and (2) multiple illumination beams to unambiguously determine Doppler angle by comparing the flow measurements from different directions. Using these techniques, a reduced retinal blood flow has been detected in glaucomatous eyes that corresponded with locations of visual field damage [88, 89]. Investigators are also actively investigating the use of Doppler OCT to measure neurovascular coupling [90], which is thought to be disturbed in subjects with diabetes as well as glaucoma.

OCT angiography (Fig. 2.20), aims to contrast moving blood vessels against static tissue. The general concept behind this method is that regions that are moving (i.e., regions with blood flow) when the same region is scanned repeatedly, will be different from scan to scan (decorrelated). This decorrelation is then used to create a depth resolved map of the vasculature of the eye. Different algorithms are used by the various manufacturer to perform OCT angiography, including intensity based

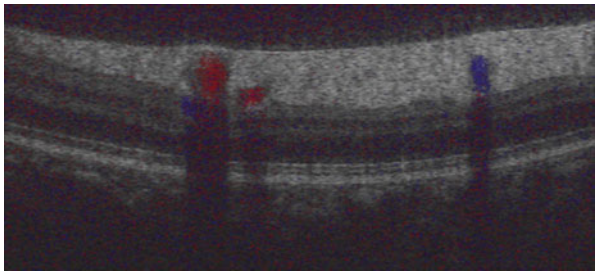

Fig. 2.19 Doppler OCT retina cross-section. The red and blue regions mark locations where blood flows toward or away from the scanning path

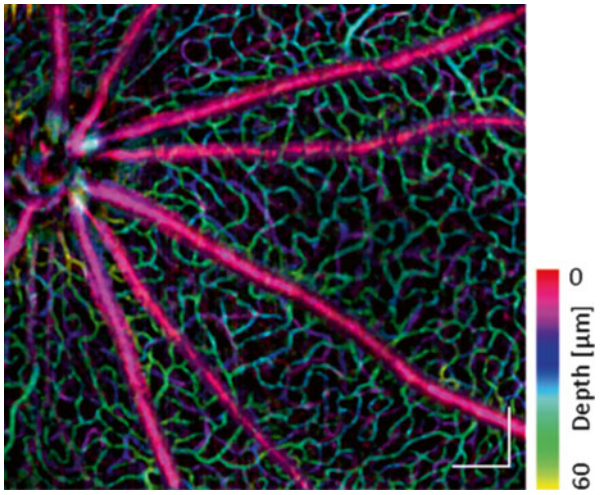

Fig. 2.20 OCT angiography of the peripapillary region in rat. Retinal vessels are color coded with depth showing large vessels on the retinal surface and fine vascular network in the inner retina (Image courtesy of W Liu and H Zhang, Functional Optical Imaging Laboratory, Department of Biomedical Engineering, Northwestern University, Evanston, IL. Scale bar: 200 µm)

and phase based algorithms. OCT angiography has benefited from the increase in OCT imaging speed, which permit imaging of flow in small capillaries as well as wide field OCT angiography [91]. The modality is most promising for assessment of various retinal pathologies involving alterations in the vasculature such as diabetic retinopathy and macular degeneration, where retinal and choroid vasculature can be evaluated with capillary level resolution [91, 92].

It should be noted that while OCT can provide high quality Doppler and angiography information, the technology is not capable of capturing leakage or blood pooling.

2.10 Phase Sensitive OCT

The Phase Sensitive OCT technique is able to provide in vivo information on micron scale movements or vibrations within the tissue [93]. The technology analyzes the phase information of the back-reflected light beam, which is typically ignored in conventional OCT systems. OCT phase imaging has been demonstrated with SD [94] and SS [95] technologies. Phase sensitive OCT offers the advantage of simultaneously assessing both the structural and functional information of the scanned tissue.

In conclusion, OCT has an important clinical role in the diagnosis of disease and the tracking of changes overtime, leading to better insight into the pathophysiology of diseases. The constant improvement in this technology ensures that clinicians will have an indispensible diagnostic tool in their armamentum.

References

1. Fujimoto JG, Brezinski ME, Tearney GJ, Boppart SA, Bouma B, Hee MR, et al. Optical biopsy and imaging using optical coherence tomography. Nat Med. 1995;1(9):970–2.
2. Fercher AF, Mengedoht K, Werner W. Eye-length measurement by interferometry with partially coherent light. Opt Lett. 1988;13(3):186–8.
3. Brezinski ME, Tearney GJ, Bouma BE, Izatt JA, Hee MR, Swanson EA, et al. Optical coherence tomography for optical biopsy. Properties and demonstration of vascular pathology. Circulation. 1996;93(6):1206–13.
4. Cobb MJ, Chen Y, Underwood RA, Usui ML, Olerud J, Li X. Noninvasive assessment of cutaneous wound healing using ultrahigh-resolution optical coherence tomography. J Biomed Opt. 2006;11(6):064002.
5. Hsiung P-L, Phatak DR, Chen Y, Aguirre AD, Fujimoto JG, Connolly JL. Benign and malignant lesions in the human breast depicted with ultrahigh resolution and three-dimensional optical coherence tomography. Radiology. 2007;244(3):865–74.
6. Chen Y, Andrews PM, Aguirre AD, Schmitt JM, Fujimoto JG. High-resolution three-dimensional optical coherence tomography imaging of kidney microanatomy ex vivo. J Biomed Opt. 2007;12(3):034008.
7. Gambichler T, Regeniter P, Bechara FG, Orlikov A, Vasa R, Moussa G, et al. Characterization of benign and malignant melanocytic skin lesions using optical coherence tomography in vivo. J Am Acad Dermatol. 2007;57(4):629–37.
8. Vincent KL, Vargas G, Wei J, Bourne N, Motamedi M. Monitoring vaginal epithelial thickness changes noninvasively in sheep using optical coherence tomography. Am J Obstet Gynecol. 2013;208(4):282.e1–7.
9. Boone M, Draye JP, Verween G, Pirnay J-P, Verbeken G, De Vos D, et al. Real-time three-dimensional imaging of epidermal splitting and removal by high-definition optical coherence tomography. Exp Dermatol. 2014;23(10):725–30.
10. Izatt JA, Hee MR, Swanson EA, Lin CP, Huang D, Schuman JS, et al. Micrometer-scale resolution imaging of the anterior eye in vivo with optical coherence tomography. Arch Ophthalmol. 1994;112(12):1584–9.
11. Puliafito CA, Hee MR, Lin CP, Reichel E, Schuman JS, Duker JS, et al. Imaging of macular diseases with optical coherence tomography. Ophthalmology. 1995;102(2):217–29.
12. Hee MR, Izatt JA, Swanson EA, Huang D, Schuman JS, Lin CP, et al. Optical coherence tomography of the human retina. Arch Ophthalmol. 1995;113(3):325–32.
13. Schuman JS, Hee MR, Arya AV, Pedut-Kloizman T, Puliafito CA, Fujimoto JG, et al. Optical coherence tomography: a new tool for glaucoma diagnosis. Curr Opin Ophthalmol. 1995;6(2):89–95.
14. Schuman JS, Hee MR, Puliafito CA, Wong C, Pedut-Kloizman T, Lin CP, et al. Quantification of nerve fiber layer thickness in normal and glaucomatous eyes using optical coherence tomography. Arch Ophthalmol. 1995;113(5):586–96.
15. Potsaid B, Gorczynska I, Srinivasan VJ, Chen Y, Jiang J, Cable A, et al. Ultrahigh speed spectral / Fourier domain OCT ophthalmic imaging at 70,000 to 312,500 axial scans per second. Opt Express. 2008;16(19):15149–69.
16. Wieser W, Biedermann BR, Klein T, Eigenwillig CM, Huber R. Multi-megahertz OCT: high quality 3D imaging at 20 million a-scans and 4.5 GVoxels per second. Opt Express. 2010;18(14):14685–704.
17. Potsaid B, Baumann B, Huang D, Barry S, Cable AE, Schuman JS, et al. Ultrahigh speed 1050 nm swept source/Fourier domain OCT retinal and anterior segment imaging at 100,000 to 400,000 axial scans per second. Opt Express. 2010;18(19):20029–48.
18. Kocaoglu OP, Cense B, Jonnal RS, Wang Q, Lee S, Gao W, et al. Imaging retinal nerve fiber bundles using optical coherence tomography with adaptive optics. Vision Res. 2011;51(16):1835–44.

19. Kuroda H, Baba M, Suzuki M, Yoneya S. A high speed three-dimensional spectral domain optical coherence tomography with <2 μm axial resolution using wide bandwidth femtosecond mode-locked laser. Appl Phys Lett. 2013;102(25):251102.
20. Fercher AF, Hitzenberger CK, Drexler W, Kamp G, Sattmann H. In vivo optical coherence tomography. Am J Ophthalmol. 1993;116(1):113–4.
21. Fercher AF, Hitzenberger CK, Kamp G, El-Zaiat SY. Measurement of intraocular distances by backscattering spectral interferometry. Opt Commun. 1995;117(1–2):43–8.
22. Wojtkowski M, Leitgeb R, Kowalczyk A, Bajraszewski T, Fercher AF. In vivo human retinal imaging by Fourier domain optical coherence tomography. J Biomed Opt. 2002;7(3):457–63.
23. Fujimoto JG. Optical coherence tomography for ultrahigh resolution in vivo imaging. Nat Biotechnol. 2003;21(11):1361–7.
24. Kim JS, Ishikawa H, Sung KR, Xu J, Wollstein G, Bilonick RA, et al. Retinal nerve fibre layer thickness measurement reproducibility improved with spectral domain optical coherence tomography. Br J Ophthalmol. 2009;93(8):1057–63.
25. Ahlers C, Schmidt-Erfurth U. Three-dimensional high resolution OCT imaging of macular pathology. Opt Express. 2009;17(5):4037–45.
26. Drexler W, Morgner U, Kärtner FX, Pitris C, Boppart SA, Li XD, et al. In vivo ultrahigh-resolution optical coherence tomography. Opt Lett. 1999;24(17):1221–3.
27. Lim H, Jiang Y, Wang Y, Huang Y-C, Chen Z, Wise FW. Ultrahigh-resolution optical coherence tomography with a fiber laser source at 1 microm. Opt Lett. 2005;30(10):1171–3.
28. Leitgeb R, Hitzenberger CK, Fercher AF. Performance of fourier domain vs. time domain optical coherence tomography. Opt Express. 2003;11(8):889–94.
29. Huber R, Adler DC, Fujimoto JG. Buffered Fourier domain mode locking: unidirectional swept laser sources for optical coherence tomography imaging at 370,000 lines/s. Opt Lett. 2006;31(20):2975–7.
30. Yaqoob Z, Wu J, Yang C. Spectral domain optical coherence tomography: a better OCT imaging strategy. Biotechniques. 2005;39(6 Suppl):S6–13.
31. Unterhuber A, Povazay B, Hermann B, Sattmann H, Chavez-Pirson A, Drexler W. In vivo retinal optical coherence tomography at 1040 nm – enhanced penetration into the choroid. Opt Express. 2005;13(9):3252–8.
32. Yasuno Y, Hong Y, Makita S, Yamanari M, Akiba M, Miura M, et al. In vivo high-contrast imaging of deep posterior eye by 1-um swept source optical coherence tomography andscattering optical coherence angiography. Opt Express. 2007;15(10):6121–39.
33. Hale GM, Querry MR. Optical constants of water in the 200-nm to 200-?m wavelength region. Appl Opt. 1973;12(3):555–63.
34. Huang D, Swanson EA, Lin CP, Schuman JS, Stinson WG, Chang W, et al. Optical coherence tomography. Science. 1991;254(5035):1178–81.
35. Schuman JS, Pedut-Kloizman T, Hertzmark E, Hee MR, Wilkins JR, Coker JG, et al. Reproducibility of nerve fiber layer thickness measurements using optical coherence tomography. Ophthalmology. 1996;103(11):1889–98.
36. Otani T, Kishi S, Maruyama Y. Patterns of diabetic macular edema with optical coherence tomography. Am J Ophthalmol. 1999;127(6):688–93.
37. Sánchez-Tocino H, Alvarez-Vidal A, Maldonado MJ, Moreno-Montañés J, García-Layana A. Retinal thickness study with optical coherence tomography in patients with diabetes. Invest Ophthalmol Vis Sci. 2002;43(5):1588–94.
38. Medeiros FA, Zangwill LM, Bowd C, Weinreb RN. Comparison of the GDx VCC scanning laser polarimeter, HRT II confocal scanning laser ophthalmoscope, and stratus OCT optical coherence tomograph for the detection of glaucoma. Arch Ophthalmol. 2004;122(6):827–37.
39. Paunescu LA, Schuman JS, Price LL, Stark PC, Beaton S, Ishikawa H, et al. Reproducibility of nerve fiber thickness, macular thickness, and optic nerve head measurements using StratusOCT. Invest Ophthalmol Vis Sci. 2004;45(6):1716–24.
40. Kamppeter BA, Schubert KV, Budde WM, Degenring RF, Jonas JB. Optical coherence tomography of the optic nerve head: interindividual reproducibility. J Glaucoma. 2006;15(3):248–54.

41. Nassif N, Cense B, Park BH, Yun SH, Chen TC, Bouma BE, et al. In vivo human retinal imaging by ultrahigh-speed spectral domain optical coherence tomography. Opt Lett. 2004;29(5):480–2.
42. Drexler W, Morgner U, Ghanta RK, Kärtner FX, Schuman JS, Fujimoto JG. Ultrahigh-resolution ophthalmic optical coherence tomography. Nat Med. 2001;7(4):502–7.
43. Ko TH, Fujimoto JG, Duker JS, Paunescu LA, Drexler W, Baumal CR, et al. Comparison of ultrahigh- and standard-resolution optical coherence tomography for imaging macular hole pathology and repair. Ophthalmology. 2004;111(11):2033–43.
44. De Boer JF, Milner TE, van Gemert MJC, Nelson JS. Two-dimensional birefringence imaging in biological tissue by polarization-sensitive optical coherence tomography. Opt Lett. 1997;22(12):934–6.
45. Izatt JA, Kulkarni MD, Yazdanfar S, Barton JK, Welch AJ. In vivo bidirectional color Doppler flow imaging of picoliter blood volumes using optical coherence tomography. Opt Lett. 1997;22(18):1439–41.
46. Bizheva K, Pflug R, Hermann B, Povazay B, Sattmann H, Qiu P, et al. Optophysiology: depth-resolved probing of retinal physiology with functional ultrahigh-resolution optical coherence tomography. Proc Natl Acad Sci U S A. 2006;103(13):5066–71.
47. Srinivasan VJ, Wojtkowski M, Fujimoto JG, Duker JS. In vivo measurement of retinal physiology with high-speed ultrahigh-resolution optical coherence tomography. Opt Lett. 2006;31(15):2308–10.
48. Kagemann L, Wollstein G, Wojtkowski M, Ishikawa H, Townsend KA, Gabriele ML, et al. Spectral oximetry assessed with high-speed ultra-high-resolution optical coherence tomography. J Biomed Opt. 2007;12(4):041212.
49. Gotzinger E, Pircher M, Baumann B, Ahlers C, Geitzenauer W, Schmidt-Erfurth U, et al. Three-dimensional polarization sensitive OCT imaging and interactive display of the human retina. Opt Express. 2009;17(5):4151–65.
50. Yamanari M, Makita S, Lim Y, Yasuno Y. Full-range polarization-sensitive swept-source optical coherence tomography by simultaneous transversal and spectral modulation. Opt Express. 2010;18(13):13964–80.
51. Cheong W-F, Prahl SA, Welch AJ. A review of the optical properties of biological tissues. IEEE J Quan Elec. 1990;26(12):2166–85.
52. Wojtkowski M, Srinivasan V, Fujimoto JG, Ko T, Schuman JS, Kowalczyk A, et al. Three-dimensional retinal imaging with high-speed ultrahigh-resolution optical coherence tomography. Ophthalmology. 2005;112(10):1734–46.
53. Leung CK-S, Cheung CY-L, Weinreb RN, Qiu Q, Liu S, Li H, et al. Retinal nerve fiber layer imaging with spectral-domain optical coherence tomography: a variability and diagnostic performance study. Ophthalmology. 2009;116(7):1257–63, 1263.e1–2.
54. Tan O, Li G, Lu AT-H, Varma R, Huang D. Advanced imaging for glaucoma study group. Mapping of macular substructures with optical coherence tomography for glaucoma diagnosis. Ophthalmology. 2008;115(6):949–56.
55. Asrani S, Rosdahl JA, Allingham RR. Novel software strategy for glaucoma diagnosis: asymmetry analysis of retinal thickness. Arch Ophthalmol. 2011;129(9):1205–11.
56. Tan O, Chopra V, Lu AT-H, Schuman JS, Ishikawa H, Wollstein G, et al. Detection of macular ganglion cell loss in glaucoma by Fourier-domain optical coherence tomography. Ophthalmology. 2009;116(12):2305–14.e1–2.
57. Margolis R, Spaide RF. A pilot study of enhanced depth imaging optical coherence tomography of the choroid in normal eyes. Am J Ophthalmol. 2009;147(5):811–5.
58. Silverman AL, Tatham AJ, Medeiros FA, Weinreb RN. Assessment of optic nerve head drusen using enhanced depth imaging and swept source optical coherence tomography. J Neuroophthalmol. 2014;34(2):198–205.
59. Park H-YL, Shin H-Y, Park CK. Imaging the posterior segment of the eye using swept-source optical coherence tomography in myopic glaucoma eyes: comparison with enhanced-depth imaging. Am J Ophthalmol. 2014;157(3):550–7.
60. Liu B, Brezinski ME. Theoretical and practical considerations on detection performance of time domain, Fourier domain, and swept source optical coherence tomography. J Biomed Opt. 2007;12(4):044007.

61. Hirata M, Tsujikawa A, Matsumoto A, Hangai M, Ooto S, Yamashiro K, et al. Macular choroidal thickness and volume in normal subjects measured by swept-source optical coherence tomography. Invest Ophthalmol Vis Sci. 2011;52(8):4971–8.
62. Adhi M, Liu JJ, Qavi AH, Grulkowski I, Lu CD, Mohler KJ, et al. Choroidal analysis in healthy eyes using swept-source optical coherence tomography compared to spectral domain optical coherence tomography. Am J Ophthalmol. 2014;157(6):1272–81.e1.
63. Takayama K, Hangai M, Kimura Y, Morooka S, Nukada M, Akagi T, et al. Three-dimensional imaging of lamina cribrosa defects in glaucoma using swept-source optical coherence tomography. Invest Ophthalmol Vis Sci. 2013;54(7):4798–807.
64. Wang B, Nevins JE, Nadler Z, Wollstein G, Ishikawa H, Bilonick RA, et al. Reproducibility of in-vivo OCT measured three-dimensional human lamina cribrosa microarchitecture. PLoS One. 2014;9(4):e95526.
65. Mak H, Xu G, Leung CK-S. Imaging the iris with swept-source optical coherence tomography: relationship between iris volume and primary angle closure. Ophthalmology. 2013;120(12):2517–24.
66. Srinivasan VJ, Adler DC, Chen Y, Gorczynska I, Huber R, Duker JS, et al. Ultrahigh-speed optical coherence tomography for three-dimensional and en face imaging of the retina and optic nerve head. Invest Ophthalmol Vis Sci. 2008;49(11):5103–10.
67. Keane PA, Ruiz-Garcia H, Sadda SR. Clinical applications of long-wavelength (1,000-nm) optical coherence tomography. Ophthalmic Surg Lasers Imaging. 2011;42(Suppl):S67–74.
68. Mishima K, Tomidokoro A, Suramethakul P, Mataki N, Kurita N, Mayama C, et al. Iridotrabecular contact observed using anterior segment three-dimensional OCT in eyes with a shallow peripheral anterior chamber. Invest Ophthalmol Vis Sci. 2013;54(7):4628–35.
69. Wang B, Nevins JE, Nadler Z, Wollstein G, Ishikawa H, Bilonick RA, et al. In vivo lamina cribrosa micro-architecture in healthy and glaucomatous eyes as assessed by optical coherence tomography. Invest Ophthalmol Vis Sci. 2013;54(13):8270–4.
70. Lopilly Park H-Y, Lee NY, Choi JA, Park CK. Measurement of scleral thickness using swept-source optical coherence tomography in patients with open-angle glaucoma and myopia. Am J Ophthalmol. 2014;157(4):876–84.
71. Považay B, Hermann B, Hofer B, Kajić V, Simpson E, Bridgford T, et al. Wide-field optical coherence tomography of the choroid in vivo. Invest Ophthalmol Vis Sci. 2009;50(4):1856–63.
72. Grulkowski I, Liu JJ, Potsaid B, Jayaraman V, Lu CD, Jiang J, et al. Retinal, anterior segment and full eye imaging using ultrahigh speed swept source OCTwith vertical-cavity surface emitting lasers. Biomed Opt Express. 2012;3(11):2733–51.
73. Liang J, Williams DR, Miller DT. Supernormal vision and high-resolution retinal imaging through adaptive optics. J Opt Soc Am A. 1997;14(11):2884–92.
74. Roorda A, Romero-Borja F, Donnelly WI, Queener H, Hebert T, Campbell M. Adaptive optics scanning laser ophthalmoscopy. Opt Express. 2002;10(9):405–12.
75. Hermann B, Fernández EJ, Unterhuber A, Sattmann H, Fercher AF, Drexler W, et al. Adaptive-optics ultrahigh-resolution optical coherencetomography. Opt Lett. 2004;29(18):2142–4.
76. Zawadzki RJ, Jones SM, Olivier SS, Zhao M, Bower BA, Izatt JA, et al. Adaptive-optics optical coherence tomography for high-resolution and high-speed 3D retinal in vivo imaging. Opt Express. 2005;13(21):8532–46.
77. Kocaoglu OP, Lee S, Jonnal RS, Wang Q, Herde AE, Derby JC, et al. Imaging cone photoreceptors in three dimensions and in time using ultrahigh resolution optical coherence tomography with adaptive optics. Biomed Opt Express. 2011;2(4):748–63.
78. Takayama K, Ooto S, Hangai M, Ueda-Arakawa N, Yoshida S, Akagi T, et al. High-resolution imaging of retinal nerve fiber bundles in glaucoma using adaptive optics scanning laser ophthalmoscopy. Am J Ophthalmol. 2013;155(5):870–81.
79. Burns SA, Tumbar R, Elsner AE, Ferguson D, Hammer DX. Large-field-of-view, modular, stabilized, adaptive-optics-based scanning laser ophthalmoscope. J Opt Soc Am A Opt Image Sci Vis. 2007;24(5):1313–26.
80. Fernández EJ, Povazay B, Hermann B, Unterhuber A, Sattmann H, Prieto PM, et al. Three-dimensional adaptive optics ultrahigh-resolution optical coherence tomography using a liquid crystal spatial light modulator. Vision Res. 2005;45(28):3432–44.

81. Zawadzki RJ, Choi SS, Fuller AR, Evans JW, Hamann B, Werner JS. Cellular resolution volumetric in vivo retinal imaging with adaptive optics-optical coherence tomography. Opt Express. 2009;17(5):4084–94.
82. Cense B, Gao W, Brown JM, Jones SM, Jonnal RS, Mujat M, et al. Retinal imaging with polarization-sensitive optical coherence tomography and adaptive optics. Opt Express. 2009;17(24):21634–51.
83. Liu S, Wang B, Yin B, Milner TE, Markey MK, McKinnon SJ, et al. Retinal nerve fiber layer reflectance for early glaucoma diagnosis. J Glaucoma. 2014;23(1):e45–52.
84. Baumann B, Rauscher S, Glösmann M, Götzinger E, Pircher M, Fialova S, et al. Peripapillary rat sclera investigated in vivo with polarization sensitive optical coherence tomography. Invest Ophthalmol Vis Sci. 2014;55(11):7686–96.
85. Michels S, Pircher M, Geitzenauer W, Simader C, Götzinger E, Findl O, et al. Value of polarisation-sensitive optical coherence tomography in diseases affecting the retinal pigment epithelium. Br J Ophthalmol. 2008;92(2):204–9.
86. Ahlers C, Götzinger E, Pircher M, Golbaz I, Prager F, Schütze C, et al. Imaging of the retinal pigment epithelium in age-related macular degeneration using polarization-sensitive optical coherence tomography. Invest Ophthalmol Vis Sci. 2010;51(4):2149–57.
87. Leitgeb RA, Werkmeister RM, Blatter C, Schmetterer L. Doppler optical coherence tomography. Prog Retin Eye Res. 2014;41:26–43.
88. Jia Y, Wei E, Wang X, et al. Optical coherence tomography angiography of optic disc perfusion in glaucoma. Ophthalmology. 2014;121(7):1322–32.
89. Sehi M, Goharian I, Konduru R, et al. Retinal blood flow in glaucomatous eyes with single-hemifield damage. Ophthalmology. 2014;121(3):750–8.
90. Wang Y, Fawzi AA, Tan O, Zhang X, Huang D. Flicker-induced changes in retinal blood flow assessed by Doppler optical coherence tomography. Biomed Opt Express. 2011;2(7):1852.
91. Blatter C, Klein T, Grajciar B, et al. Ultrahigh-speed non-invasive widefield angiography. J Biomed Opt. 2012;17(7):0705051–3.
92. Cheung CY-L, Lamoureux E, Ikram MK, et al. Retinal vascular geometry in Asian persons with diabetes and retinopathy. J Diabetes Sci Technol. 2012;6(3):595–605.
93. Choma MA, Ellerbee AK, Yang C, Creazzo TL, Izatt JA. Spectral-domain phase microscopy. Opt Lett. 2005;30(10):1162–4.
94. Joo C, Akkin T, Cense B, Park BH, de Boer JF. Spectral-domain optical coherence phase microscopy for quantitative phase-contrast imaging. Opt Lett. 2005;30(16):2131–3.
95. Sarunic MV, Weinberg S, Izatt JA. Full-field swept-source phase microscopy. Opt Lett. 2006;31(10):1462–4.